

Supplementary Information

Allometric Scaling and Resource Limitations Model of Tree Heights: Part 2. Site Based Testing of the Model. *Remote Sens.* 2013, 5, 202–223

Sungho Choi^{1,*†}, **Xiliang Ni**^{1,2,†}, **Yuli Shi**^{1,3}, **Sangram Ganguly**⁴, **Gong Zhang**⁵, **Hieu V. Duong**⁶, **Michael A. Lefsky**⁶, **Marc Simard**⁷, **Sassan S. Saatchi**⁷, **Shihyan Lee**⁸, **Wenge Ni-Meister**⁸, **Shilong Piao**⁹, **Chunxiang Cao**², **Ramakrishna R. Nemani**¹⁰ and **Ranga B. Myneni**¹

¹ Department of Earth and Environment, Boston University, 675 Commonwealth Avenue, Boston, MA 02215, USA; E-Mail: ranga.myneni@gmail.com

² State Key Laboratory of Remote Sensing Sciences, Institute of Remote Sensing Applications, Chinese Academy of Sciences, Beijing 100101, China; E-Mails: nixl@irsa.ac.cn (X.N.); cao413@irsa.ac.cn (C.C.)

³ School of Remote Sensing, Nanjing University of Information Science and Technology, Nanjing 210044, China; E-Mail: ylshi.nuist@gmail.com

⁴ Bay Area Environmental Research Institute (BAERI)/NASA Ames Research Center, Moffett Field, CA 94035, USA; E-Mail: sangramganguly@gmail.com

⁵ Department of Watershed Science, Utah State University, UT 84322, USA; E-Mail: gongzhang07@gmail.com

⁶ Center for Ecological Analysis of Lidar, Natural Resource Ecology Laboratory, Colorado State University, Fort Collins, CO 80523, USA; E-Mails: Hieu.Duong@colostate.edu (H.D.); lefsky@cnr.colostate.edu (M.L.)

⁷ Jet Propulsion Laboratory, California Institute of Technology, 4800 Oak Grove Dr., Pasadena, CA 91109, USA; E-Mails: marc.simard@jpl.nasa.gov (M.S.); saatchi@jpl.nasa.gov (S.S.)

⁸ Department of Geography, Hunter College of CUNY, New York, NY 10065, USA; E-Mails: shihyanlee@yahoo.com (S.L.); Wenge.Ni-Meister@hunter.cuny.edu (W.N.)

⁹ College of Urban and Environmental Sciences and Sino-French Institute for Earth System Science, Peking University, Beijing 100871, China; E-Mail: slpiao@pku.edu.cn

¹⁰ Biospheric Science Branch, NASA Ames Research Center, Moffett Field, CA 94035, USA; E-Mail: rama.nemani@nasa.gov

† These authors contributed equally to this work.

* Author to whom correspondence should be addressed; E-Mail: schoi@bu.edu; Tel.: +1-617-353-8846; Fax: +1-617-353-8399.

List of Abbreviations

ASRL	Allometric Scaling and Resource Limitations
CONUS	Continental USA
DBH	Diameter at Breast Height
DEM	Digital Elevation Model
ETM+	Enhanced Thematic Mapper+
FWHM	Full Width at Half Maximum
GLA14	GLAS Level-2 Land Surface Altimetry
GLAS	Geoscience Laser Altimeter System
ICESat	Ice, Cloud and land Elevation Satellite
LAI	Leaf Area Index
LEDAPS	Landsat Ecosystem Disturbance Adaptive Processing System
LGE	LVIS Ground Elevation
LVIS	Laser Vegetation Imaging Sensor
MODIS	Moderate Resolution Imaging Spectroradiometer
NED	National Elevation Dataset
NLCD2006	National Land Cover Database 2006
ORNL DAAC	Oak Ridge National Laboratory Distributed Active Archive Center
RMSE	Root Mean Square Error
USGS	US Geological Survey
VCF	Vegetation Continuous Fields

S1. Field Data

S1.1. La Selva Biological Station, Costa Rica

A field-measured dataset of tree heights (10 m by 100 m subplot size; N = 30) from the La Selva Biological Station located in Costa Rica was used in this study. Visual height estimation (*i.e.*, the ocular method) was used. The data were collected in February 2006 [1,2]. Tree heights with valid Diameter at Breast Height (DBH) greater than 10 cm were measured. Clinometer readings between the lowest and highest points of the canopy were applied to calibrate the measurements [1,2].

S1.2. Barro Colorado Island, Panama

The Smithsonian Tropical Research Institute has conducted census studies over a permanent tree measurement plot (50 ha) in Barro Colorado Island in central Panama since 1980 [3,4]. Amongst 50 available subplots (1 ha) in this permanent site, this study used 20 subplots that have tree heights with DBH > 10 cm. Data from the year 2000 census were used in this study [5].

S1.3. Penobscot Experimental Forest, Maine

There are approximately 580 permanent inventory plots available from the long-term database [6]. The field-measured data in August 2009 consisted of about 9000 sample trees with DBH > 10 cm over 12 subplots (1 ha; 50 m by 200 m) [7].

S1.4. ECHIDNA Lidar Campaigns Field Data from ORNL DAAC

Field-measured data of tree heights from the ECHIDNA lidar campaigns are available from the Oak Ridge National Laboratory Distributed Active Archive Center (ORNL DAAC; [8]). There are four individual sites, namely the Sierra National Forest in California (in July 2008), Harvard Forest in Massachusetts, Howland Research Forest in Maine, and the Bartlett Experimental Forest in New Hampshire (in August 2007 and in July–August 2009) [8]. Trees with DBH > 10 cm were measured over a total of 20 subplots—dimensions of the subplots are (a) 100 m by 100 m for 2007 and 2008 Campaigns and (b) 50 m by 50 m for the 2009 Campaign [9].

S2. Remote Sensing Data

S2.1. LVIS Data

Amongst the three available data types of the Laser Vegetation Imaging Sensor (LVIS) waveform data [10], the LVIS Ground Elevation (LGE) was used in this study. Raw tree height values were extracted from the LGE standard product (*i.e.*, *RH100*) using the LVIS release reader [10]. The size of LVIS footprints was assumed to be ~20 m. Topographic gradient effects were corrected with the LVIS preprocessing algorithm of Lee *et al.* [11].

S2.2. GLAS Data

Geoscience Laser Altimeter System (GLAS) waveform data should be screened for scientific analysis based on (a) data quality flags, (b) data correction factors and (c) ancillary information from other data sources, such as elevation maps and land cover data [12]. The GLAS waveform is strongly influenced by satellite orbit and attitude, atmospheric delay and forward scattering [12]; *e.g.*, the trailing edges of the GLAS waveform shift due to forward or multiple scattering from cirrus clouds. This introduces uncertainties in the Gaussian decomposition approach. This research used several preprocessing filters to screen invalid GLAS waveform data: atmospheric forward scattering and signal saturation, background noise level correction and landcover masks derived from the National Land Cover Database (NLCD) landcover and Moderate Resolution Imaging Spectroradiometer (MODIS) Vegetation Continuous Fields (VCF) product.

S2.3. Ancillary Data for GLAS and LVIS Data Preprocessing

S2.3.1. NLCD Landcover Data

The NLCD 2006 landcover data over the Continental USA (CONUS) at 30 m spatial resolution is derived from the Landsat Enhanced Thematic Mapper (ETM+) data [13,14]. Among the 16 landcover

classes provided in the NLCD, three dominant forest classes (deciduous, evergreen, and mixed forests) were selected to derive a landcover mask.

S2.3.2. MOD44B VCF Product

The Collection 5 MODIS VCF product (year 2005) is available from the US Geological Survey (USGS). The MODIS VCF currently provides estimates of percent tree cover at 250 m spatial resolution. The VCF product is derived from monthly composites of MODIS surface reflectance data based on a supervised regression tree algorithm [15]. VCF values were applied to remove invalid GLAS footprints over non-tree and/or bare ground (percent tree cover < 50%).

S2.3.3. NED DEM Data

The USGS provides the National Elevation Dataset (NED) Digital Elevation Model (DEM) data over the CONUS at a spatial resolution of 1 arc-second (~30 m). This can be converted into slope, shaded-relief and synthetic drainage information [17]. To generate a continuous field of the slope, a 3 by 3 window filter is applied to calculate the maximum rate of elevation changes between each grid cell and its corresponding neighbors, *i.e.*, the steepest downhill descent for a grid cell.

S3. GLAS Data Preprocessing

Elevations of the uppermost surface of the tree canopy and of the ground surface can be retrieved from the echo waveform of the GLAS waveform data [18]. However, laser returns of the GLAS waveform are affected by three degrading factors: (a) atmospheric forward scattering and signal saturation, (b) background noise (low cloud) and (c) slope gradient effects. Additionally, GLAS footprints over non-forest and/or bare ground must be filtered from analysis. In this study, four screening filters were applied to identify invalid GLAS waveform data prior to retrieval of tree heights. All the datasets used in the GLAS preprocessing have the same projection; Geographic Lat/Lon. GLAS footprints have a coarser spatial resolution (70 m) than ancillary datasets (e.g., NLCD and NED DEM data are at a 30 m spatial resolution). So, the values of the pixel nearest to the center of a GLAS footprint were used in this analysis.

S3.1. Atmospheric Forward Scattering and Signal Saturation Filter

Only cloud-free and saturation-free GLAS waveform data were used in this study. Internal flags of GLAS data, “*FRir_qaFlag = 15*” and “*satNdx = 0*”, remove invalid GLAS footprints affected by atmospheric forward scattering and signal saturation [19].

S3.2. NLCD and VCF Filters

NLCD and VCF filters screen invalid GLAS footprints from non-forested areas and bare ground. Using geolocation of NLCD and VCF pixels (pixels nearest to the center of a GLAS footprint), GLAS footprints over deciduous, evergreen, and mixed forests with greater than 50% of the tree cover were considered in this analysis.

S3.3. Background Noise Level (Low Cloud) Correction Filter

The NED DEM was applied to remove the background noise level (low cloud) effects prevalent in GLAS waveform data. Theoretically, laser returns cannot penetrate clouds and may record heights of low-level clouds. Hence, a filter was set to remove invalid GLAS footprints using the absolute difference (50 m) between the NED DEM and the internal elevation value from the GLAS waveform data [20].

S3.4. Slope Gradient Correction Filter

The slope generally influences the full GLAS waveform extent. It is necessary to correct the topographic gradient effects on the GLAS waveform for accurate retrieval of tree heights. The slope gradient filter is based on slope values of <5 , $5 - 10$ and $10 - 20$ over the nearest pixel from GLAS footprints [21].

S4. Five Metrics of Tree Heights from GLAS Waveform Variables

There are two approaches of retrieving tree heights from GLAS waveform data [11]. The first refers to the “*statistical analysis for examining full GLAS waveform extents*” [21–24]. The other approach is the “*Decomposition of GLAS waveforms into multiple Gaussian distribution curves*” [11,16,19,25–27]. The first approach was not considered in this study.

This study investigated the relationship between LVIS tree heights and five possible GLAS metrics representative of tree heights that can be derived by the Gaussian decomposition approach. The GLAS height metric H_A represents the distance between values of “*SigBegOff*” and “*gpCntRngOff I*” [16,26,27]. The metric H_B represents the distance between values of “*SigBegOff*” and “*SigEndOff*” from the full GLAS waveform extent [27] (Equations (S1) and (S2)). Both these metrics can be potentially affected by the topographic gradient [21].

$$H_A = H + \frac{d \times \tan \theta}{2} \quad (\text{S1})$$

$$H_B = H + d \times \tan \theta + \frac{C \times FWHM}{2} \quad (\text{S2})$$

here H is the actual forest canopy height, θ represents the slope, d refers to the diameter of a GLAS footprint (~ 70 m), C is the speed of light and $FWHM$ refers to the laser pulse width (6 ns equivalent to 1.8 m) for the GLAS waveform. The surface roughness also plays a similar role in broadening the GLAS waveform. The operation $C \times FWHM$ coherently affects the laser pulse width, energy distribution and surface roughness.

The other two GLAS height metrics (H_C and H'_D) are retrieved from H_A and H_B with correction for the topographic effect using Equations (S3) and (S4). In this study, we assumed that surface roughness conditions can be neglected (H_D converted from H'_D ; Equation (S5)). Lastly, H_E is computed from the integration of H_C and H_D regardless of the topographic gradient effect (Equation (S6)).

$$H_C = H_A - \frac{d \times \tan \theta}{2} \quad (\text{S3})$$

$$H'_D = H_B - d \times \tan \theta - \frac{C \times FWHM}{2} \quad (S4)$$

$$H_D = H_B - d \times \tan \theta \quad (S5)$$

$$H_E = 2 \times H_A - H_B \quad (S6)$$

S5. Figures S1-S10

Figure S1. Distribution of the seven field measurement sites superimposed on Landsat imagery. Red dots represent subplots. The field measurement campaigns (or census) have different acquisition dates. The size and number of subplots vary depending on the location of field sites. All the subplots have corresponding Laser Vegetation Imaging Sensor (LVIS) datasets. **(a)** La Selva Biological Station, **(b)** Barro Colorado Island, **(c)** Penobscot Experimental Forest, **(d)** Sierra National Forest, **(e)** Harvard Forest, **(f)** Howland Research Forest and **(g)** Bartlett Experimental Forest.

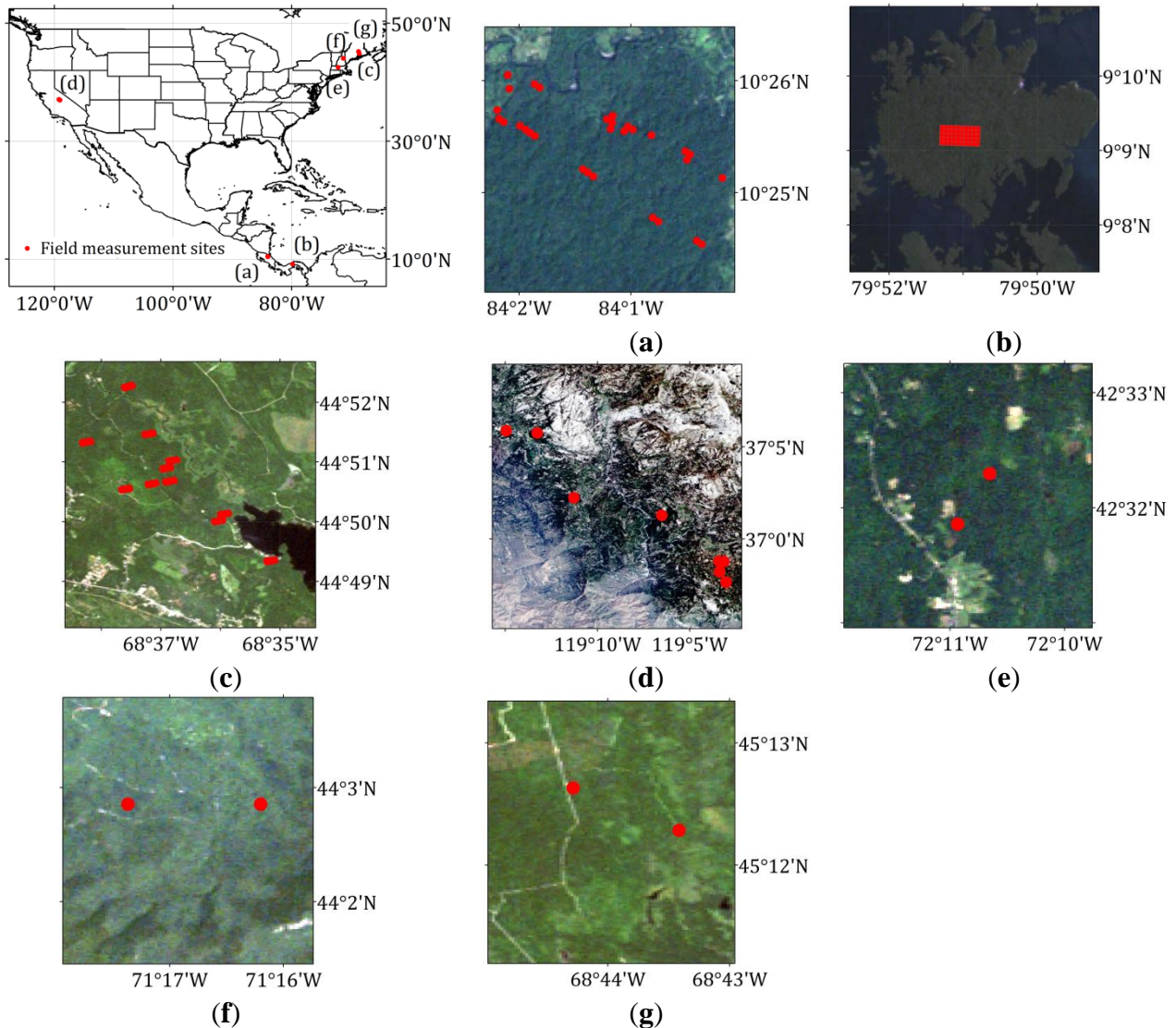


Figure S2. Distribution of Geoscience Laser Altimeter System (GLAS) footprints (colored dots) superimposed on Landsat imagery. A GLAS footprint corresponds to several LVIS footprints. Footprint sizes of GLAS and LVIS are assumed to be 70 m and 20 m, respectively. **(a)** White River Wildlife Refuge, Arkansas, **(b)** Sierra Nevada, California, **(c)** Harvard Forest, Massachusetts, **(d)** Patapsco Forest, Maryland, **(e)** Howland Research Forest and Penobscot Experimental Forest, Maine and **(f)** Bartlett Experimental Forest, New Hampshire.

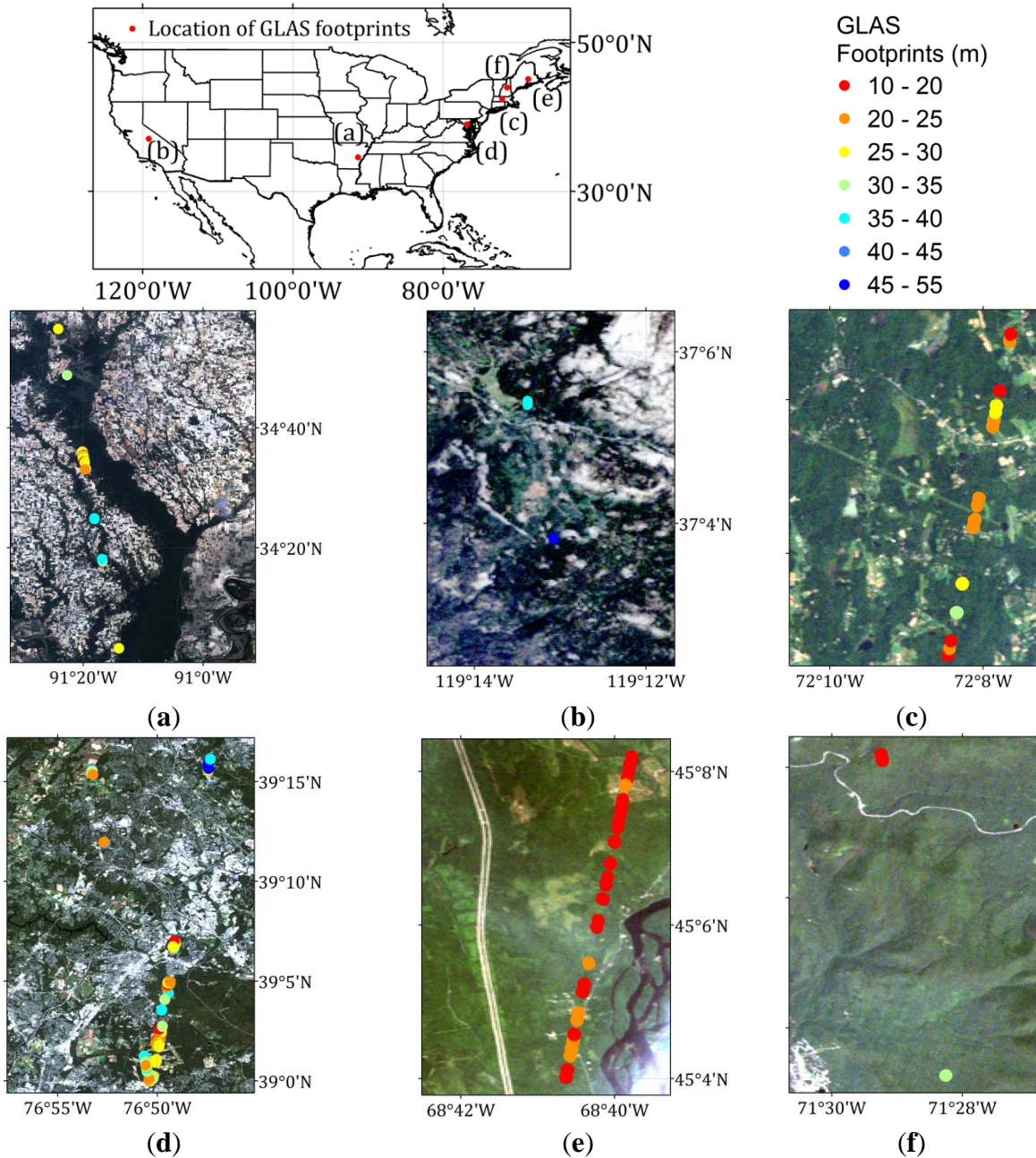


Figure S3. (a) Landcover map derived from the National Land Cover Database (NLCD) 2006 (30 m spatial resolution). The three dominant forest types over the continental USA (CONUS) are Deciduous, Evergreen and Mixed Forests (11.0%, 11.9%, and 2.1%, respectively). (b) Percent tree cover (%) derived from the Moderate Resolution Imaging Spectroradiometer Vegetation Continuous Fields (VCF) at a 250 m spatial resolution (year 2005). Forested land over the CONUS is defined using $\geq 50\%$ tree cover threshold. (c) The National Elevation Dataset (NED) Digital Elevation Model (DEM) data at 1 arc-second spatial resolution (~ 30 m). (d) Slope map generated from the NED DEM data using a 3 by 3 window filter calculating the steepest downhill descent for a grid cell.

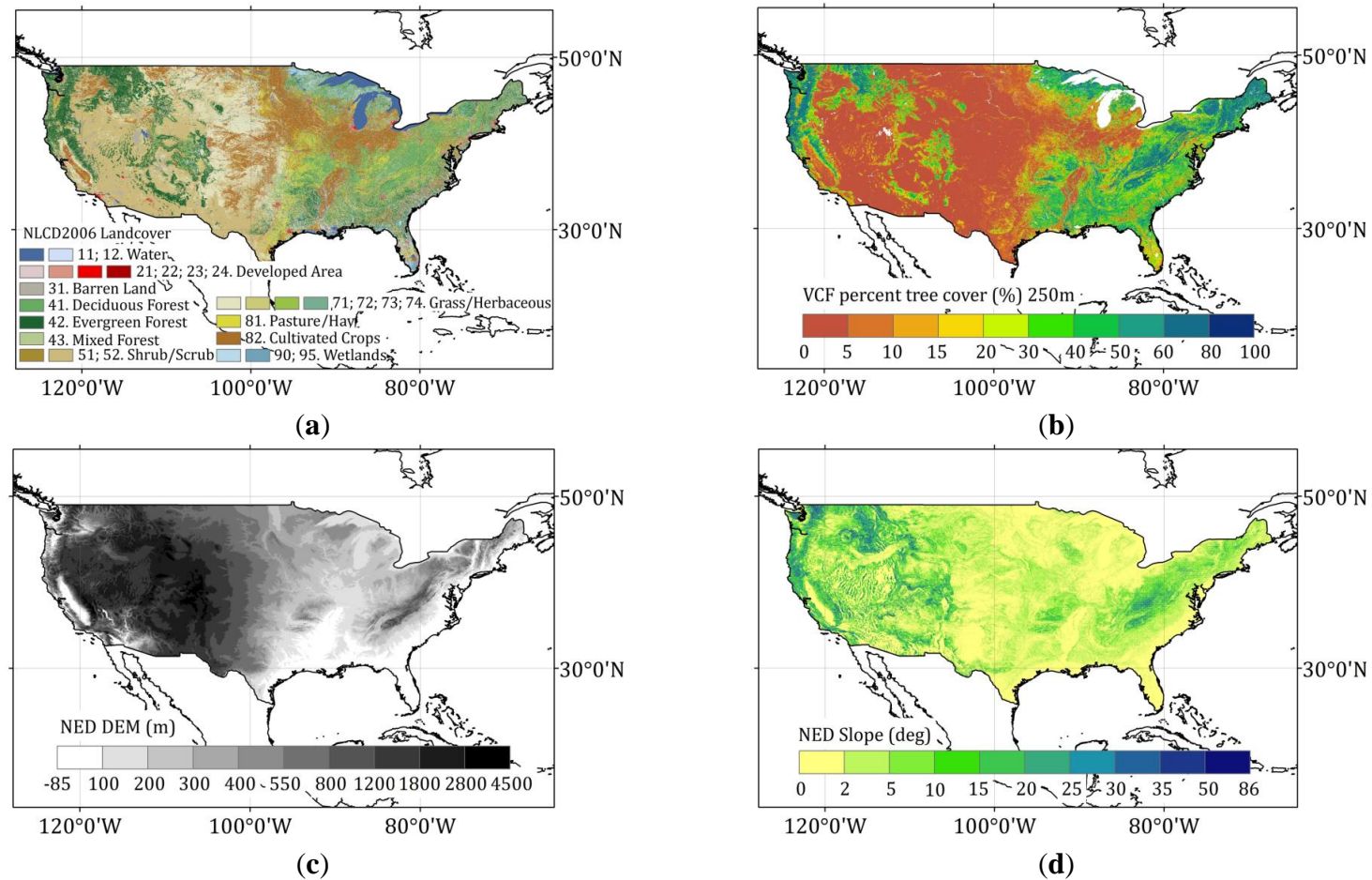


Figure S4. Schematic illustration of comparison between field-measured and LVIS tree heights. The example here shows a subplot in the Harvard Forest (plot #2; New England 2007 Campaign). The average of the top 25% of field-measured tree heights ($N_{\text{field-measured}} = 13$) is used to represent the field-measured tree height of this subplot. There are 107 LVIS footprints within this subplot. The average of the top 25% of LVIS tree heights ($N_{\text{LVIS}} = 27$) is used to represent the LVIS tree height of this subplot.

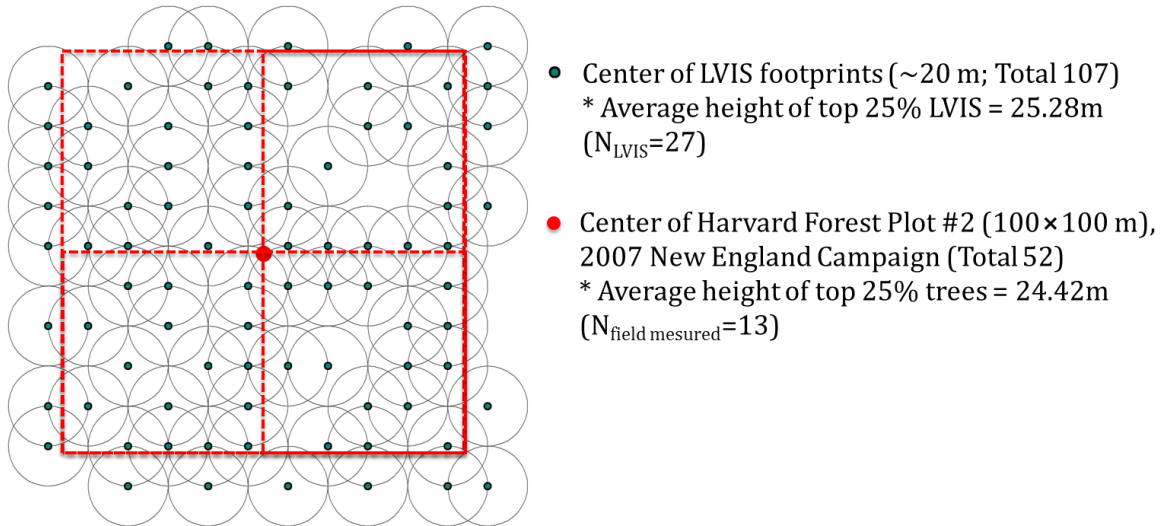


Figure S5. Comparison of LVIS and GLAS tree heights. In this example, there are 25 LVIS footprints (diameter = 20 m) that correspond to a GLAS footprint (diameter = 70 m). The average of the top 25% of LVIS tree heights is used in the comparison (the average of 6 LVIS-derived tree heights = 24.5 m). The smaller hollow circular rim resembles the LVIS footprint and the shaded inner concentric circular rim resembles the GLAS footprint (the area between the inner concentric circle and the outer circle represents a buffer zone).

Average height of
top 25% LVIS Footprints = 24.5 m (N = 6)

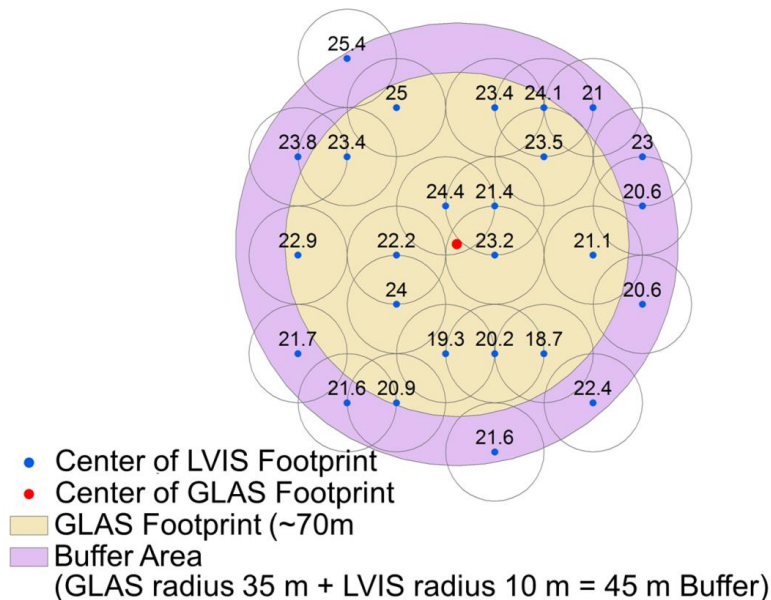


Figure S6. Distribution of the 12 selected FLUXNET sites in the precipitation and temperature space. Eco-climatic zones are defined based on dominant forest type and fixed ranges of precipitation (30 mm intervals) and temperature (2 °C intervals). Symbols with red color represent FLUXNET sites within a climatic zone. Five climatic zones satisfy the criterion that GLAS footprints be ≥ 50 .

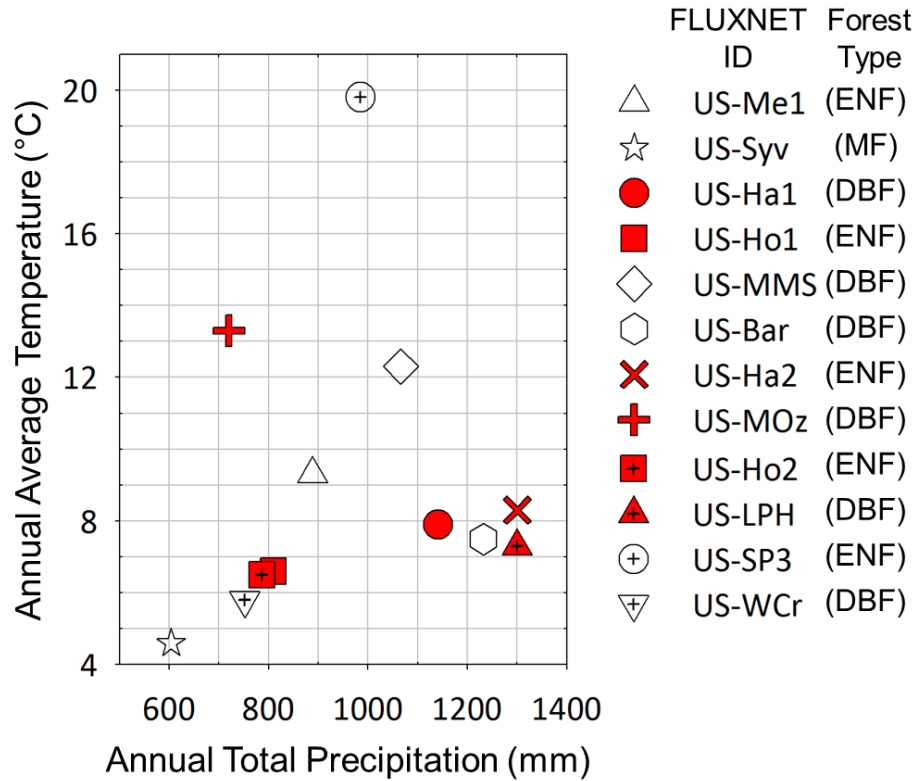


Figure S7. Comparisons between LVIS tree heights and five GLAS height metrics (H_{A-E} , Table 4). The slope of the terrain in all cases is greater than 5 degrees and less than 10 degrees.

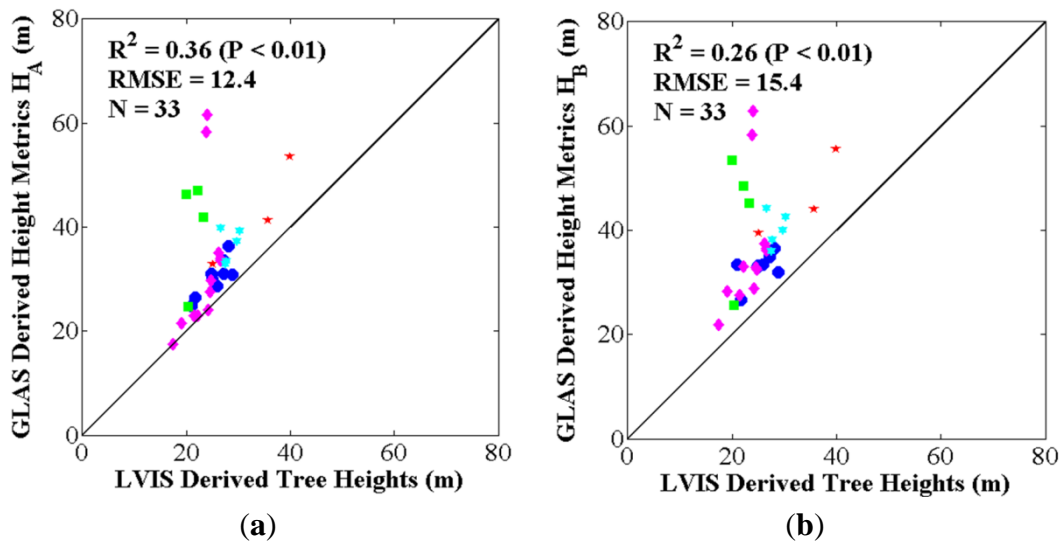


Figure S7. Cont.

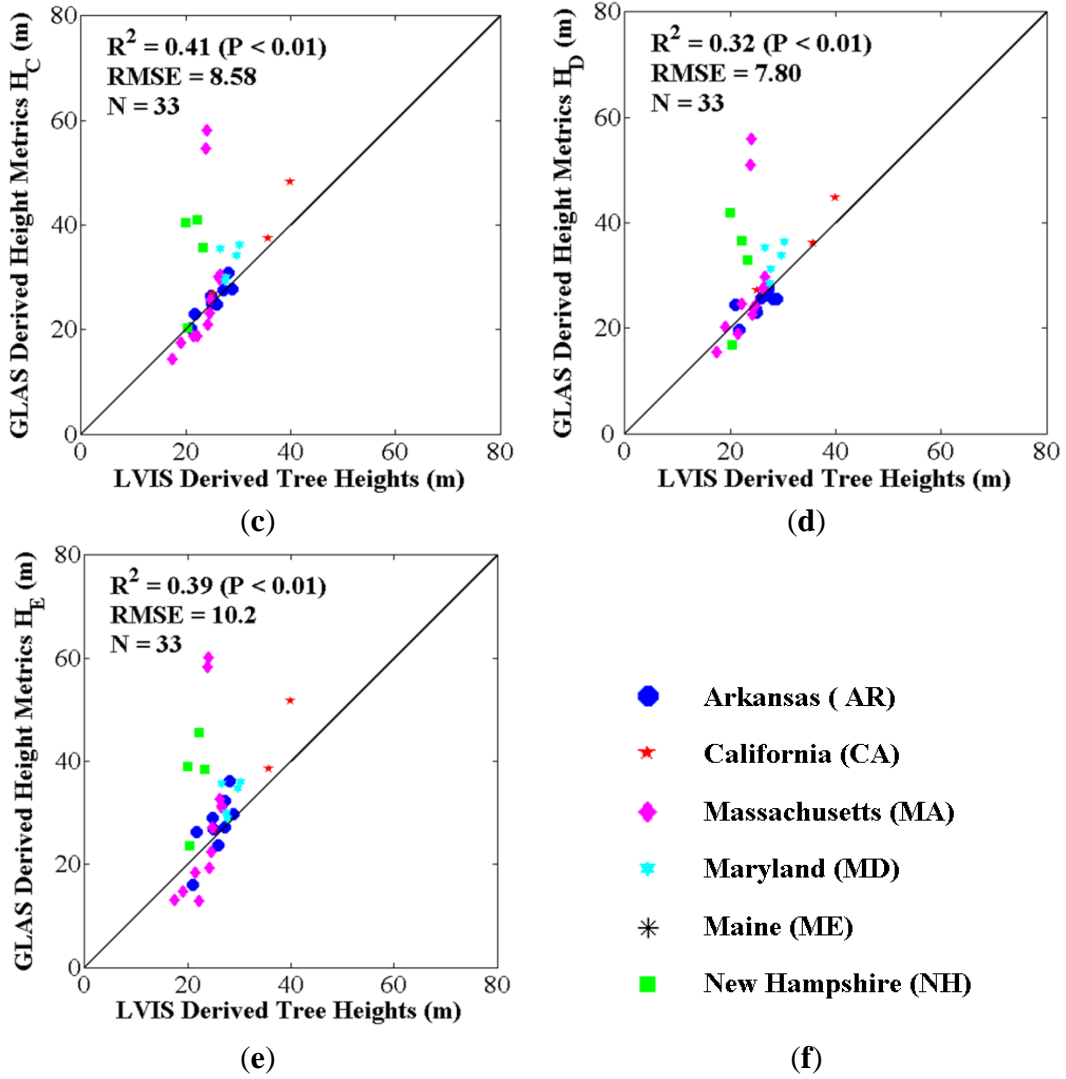


Figure S8. Comparison between LVIS tree heights and five GLAS height metrics (H_{A-E} , Table 4). The slope of the terrain in all cases is greater than 10 degrees and less than 20 degrees.

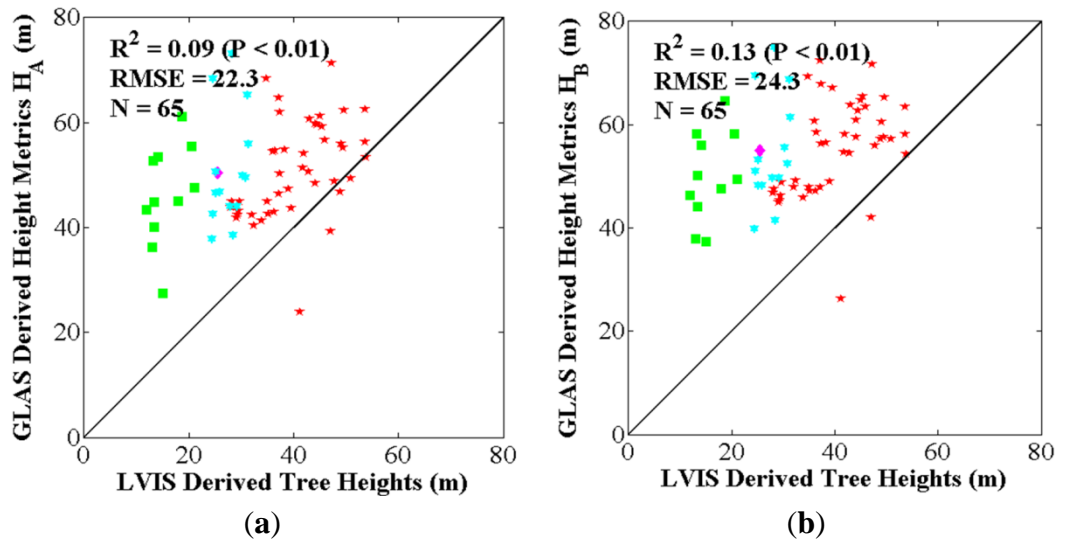


Figure S8. Cont.

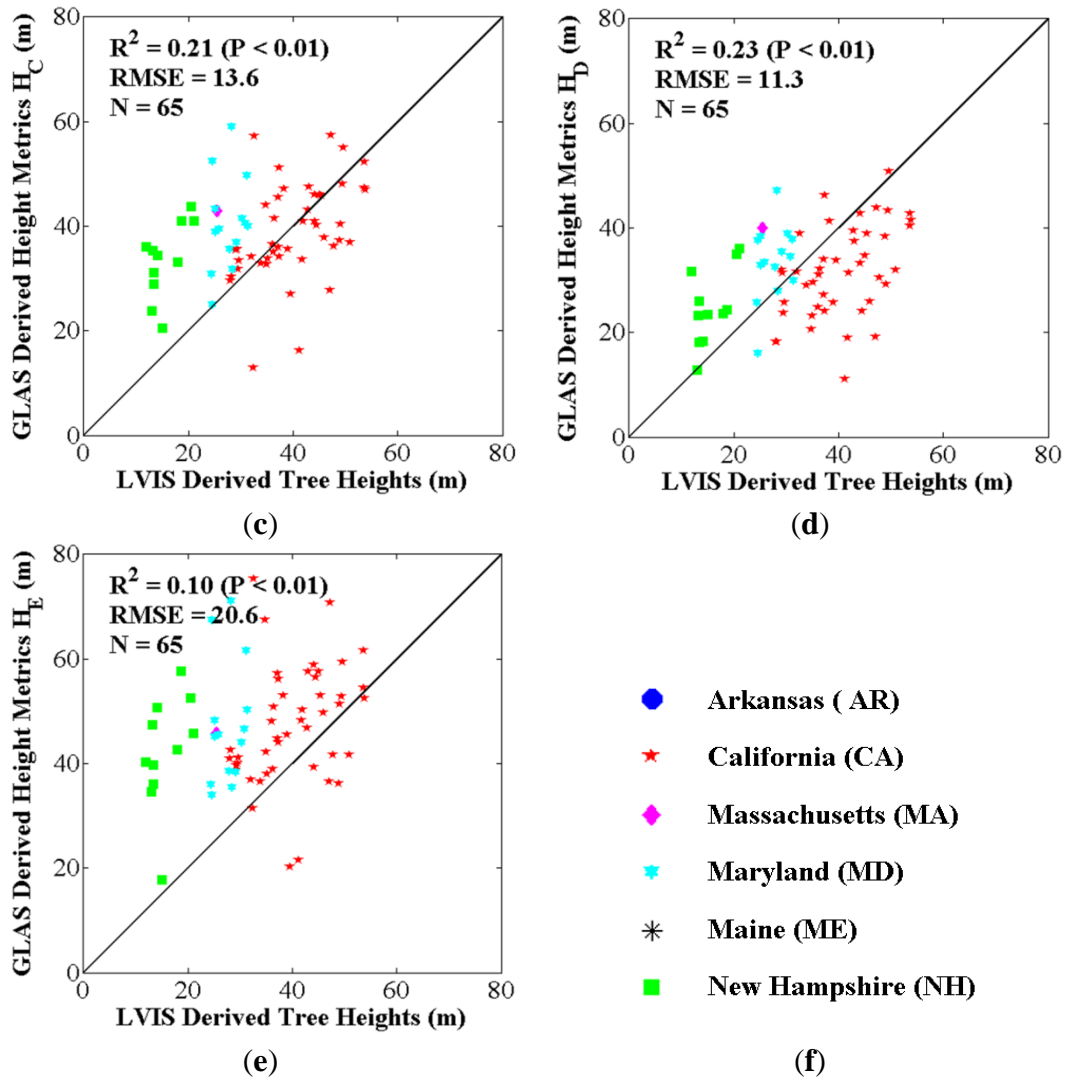


Figure S9. Improvement of the ASRL model prediction over 12 FLUXNET sites after model optimization. The variance of model errors to observation, “ $(GLAS \text{ tree heights} - \text{Predicted tree heights})/GLAS \text{ tree heights}$ ”, decreased from (a) 0.53 (without optimization) to (b) 0.01 (after optimization). This comparison is based on a two-fold cross validation approach that randomly divides GLAS tree heights into two equal sets of training and test data.

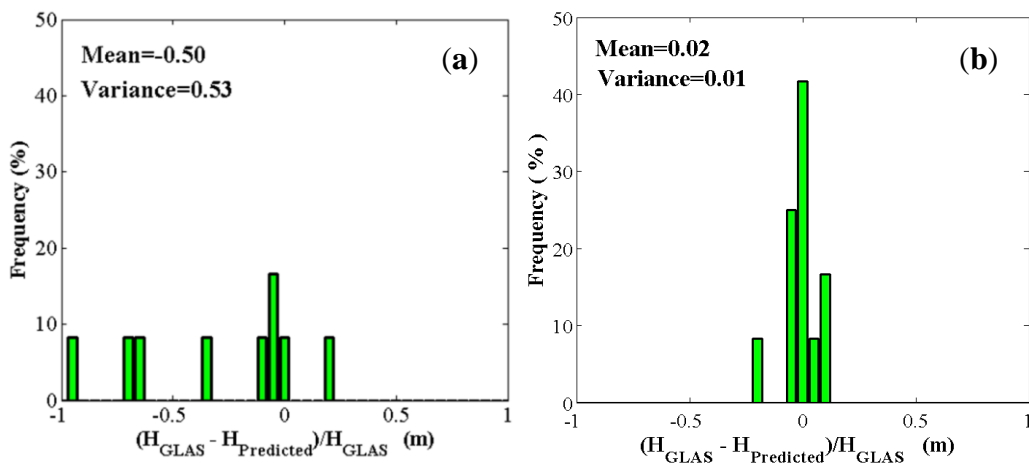
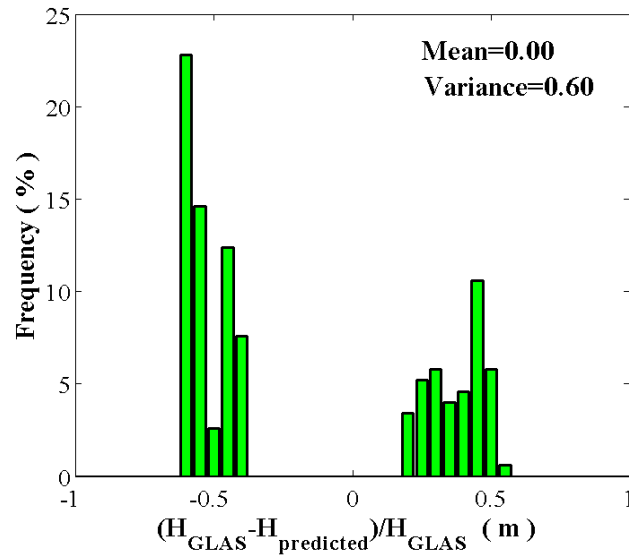
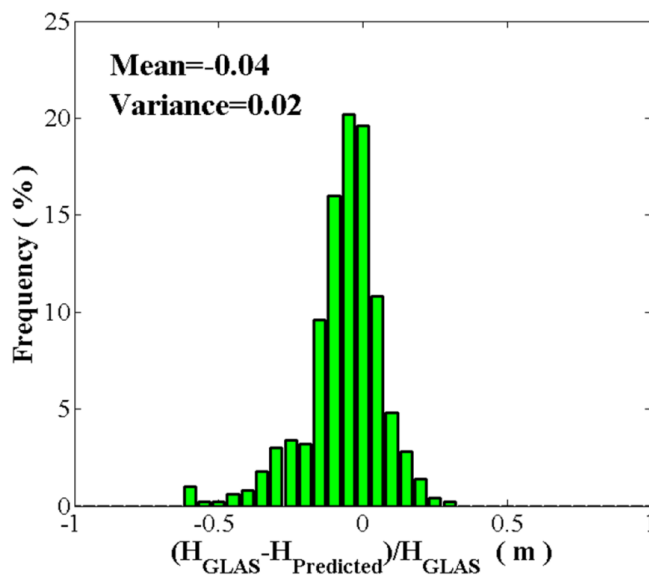


Figure S10. Improvement of the ASRL model prediction over five eco-climatic zones after model optimization. The variance of model errors to observation decreased from (a) 0.60 to (b) 0.02 after model optimization. In this bootstrapping evaluation, several FLUXNET sites were stratified into five eco-climatic zones delineated by the dominant forest type, annual total precipitation class and annual average temperature class. These five zones have more than 50 corresponding GLAS footprints.



(a)



(b)

S6. Tables S1-S3

Table S1. Input climatic and ancillary values for the initial ASRL model run. Annual total precipitation (Prec.) and annual average temperature (Temp.) values were obtained from the FLUXNET sites. FLUXNET IDs and geolocations (Lat./Lon.) are provided. Vapor pressure (Vpr.), wind speed (Wind; fixed value at 3.5m/s), and solar radiation (SRad.) values were derived from the DAYMET database. Ancillary data of Leaf Area Index (LAI) were obtained from Landsat Thematic Mapper (TM) surface reflectances (Red and NIR spectral bands referred to as Refl.B.3 and Refl.B.4 in the table) using a physically-based algorithm. The Landsat data are characterized by the TM scene path/row and the acquisition date (Acq. Date).

FLUXNET Data Specifics				DAYMET Data				Landsat Data Specifics					
ID (US-)	Lat.	Lon.	Temp. (°C)	Prec. (mm)	Vpr. (Hpa)	Wind (m/s)	SRad.	Path	Row	Acq. Date	Refl. B.3	Refl. B.4	LAI
Me1	44.6	-121.5	9.3	888.6	597.4	3.5	5.8	45	29	Jul., 06	0.092	0.160	0.3
Syv	46.2	-89.3	4.6	603.9	670.5	3.5	12.4	25	28	Jul., 03	0.027	0.443	4.2
Ha1	42.5	-72.2	7.9	1,140.8	808.3	3.5	11.2	13	30	Sep., 05	0.022	0.327	3.9
Ho1	45.2	-68.7	6.6	809.1	757.3	3.5	11.2	11	29	Jul., 05	0.022	0.265	3.4
MMS	39.3	-86.4	12.3	1,066.0	1,092.5	3.5	14.4	21	33	Jul., 03	0.024	0.387	4.2
Bar	44.1	-71.3	7.5	1,232.3	747.5	3.5	13.1	13	29	Sep., 05	0.027	0.285	3.1
Ha2	42.5	-72.2	8.3	1,300.6	806.4	3.5	9.2	13	30	Sep., 05	0.022	0.260	3.5
MOz	38.7	-92.2	13.3	720.1	1,156.4	3.5	14.8	25	33	Jul., 04	0.029	0.341	3.3
Ho2	45.2	-68.7	6.5	786.5	755.1	3.5	11.3	11	29	Jul., 05	0.026	0.275	3.2
LPH	42.5	-72.2	7.3	1,300.2	807.3	3.5	9.5	13	30	Sep., 05	0.022	0.306	3.7
SP3	29.8	-82.2	19.8	984.8	1,755.2	3.5	15.7	17	39	Jun., 05	0.058	0.266	1.5
WCr	45.8	-90.1	5.8	751.9	693.3	3.5	12.8	25	28	Jul., 03	0.023	0.403	4.3

Table S2. Five eco-climatic zones for the bootstrapping evaluation approach. The zones are defined using three dominant forest types, annual total precipitation classes and annual average temperature classes. A valid climatic zone involving 1 to 2 FLUXNET sites should have more than 50 corresponding GLAS footprints to generate 100 sets of bootstrapping subsamples. Note that US-Ho1 and US-Ho2 are aggregated into one climate zone (ID 2). Averaged input variables from the two sites are used in the ASRL model runs. DBF refers to Deciduous Broadleaf Forest and ENF represents Evergreen Needleleaf Forest.

Climatic Zone ID	Forest Type	Annul Average Temperature Range (°C)	Annul Total Precipitation Range (mm)	Corresponding FLUXNET Sites
1	DBF	7–9	1140–1170	US-Ha1
2	ENF	5–7	780–910	US-Ho1 and US-Ho2
3	ENF	7–9	1290–1320	US-Ha2
4	DBF	13–15	720–750	US-MOz
5	DBF	7–9	1290–1320	US-LPH

Table S3. Adjusted allometric parameters of the ASRL model after model optimization in the two-fold cross validation approach. Each of the FLUXNET sites consists of randomly divided two equal sets of training and test GLAS waveform data.

FLUXNET Site ID	Area of Single Leaf (α)	Exponent for Canopy Radius (η)	Root Absorption Efficiency (γ)	Number of GLAS Footprints for Training
US-Me1	18.9	1.14	0.33	15
US-Syv	27.2	1.12	0.27	17
US-Ha1	45.3	1.24	0.32	34
US-Ho1	21.2	1.18	0.19	17
US-MMS	14.0	1.16	0.32	9
US-Bar	18.3	1.14	0.24	6
US-Ha2	56.0	1.23	0.33	34
US-MOz	29.9	0.94	0.43	32
US-Ho2	19.5	1.18	0.19	16
US-LPH	24.4	1.21	0.19	34
US-SP3	26.9	1.14	0.38	15
US-WCr	20.3	1.19	0.28	5

References

1. Treuhaft, R.N.; Chapman, B.D.; dos Santos, J.R.; Gonçalves, F.G.; Dutra, L.V.; Graça, P.M.L.A.; Drake, J.B. Vegetation profiles in tropical forests from multibaseline interferometric synthetic aperture radar, field, and lidar measurements. *J. Geophys. Res.* **2009**, *114*, doi: 10.1029/2008jd011674.

2. Treuhaft, R.N.; Gonçalves, F.G.; Drake, J.B.; Chapman, B.D.; dos Santos, J.R.; Dutra, L.V.; Graça, P.M.L.A.; Purcell, G.H. Biomass estimation in a tropical wet forest using Fourier transforms of profiles from lidar or interferometric SAR. *Geophys. Res. Lett.* **2010**, *37*, doi: 10.1029/2010gl045608.
3. Condit, R. *Tropical Forest Census Plots: Methods and Results from Barro Colorado Island, Panama, and a Comparison with Other Plots*; Springer: Berlin, Germany; New York, NY, USA, 1998; p.10.
4. Hubbell, S.P.; Foster, R.B.; O'Brien, S.T.; Harms, K.E.; Condit, R.; Wechsler, B.; Wright, S.J.; de Lao, S.L. Light-gap disturbances, recruitment limitation, and tree diversity in a neotropical forest. *Science* **1999**, *283*, 554–557.
5. Hubbell, S.P.; Condit, R.; Foster, R.B. *Barro Colorado Forest Census Plot Data*; Center for Tropical Forest Science of Smithsonian Tropical Research Institute: Panama, Republic of Panama, 2005. Available online: <https://ctfs.arnarb.harvard.edu/webatlas/datasets/bci> (accessed on 15 April 2012).
6. *Penobscot Experimental Forest*. Available online: <http://www.fs.fed.us/ne/durham/4155/penobsco.htm> (accessed on 15 April 2012).
7. Cook, B.; Dubayah, R.; Hall, F.; Nelson, R.; Ranson, J.; Strahler, A.; Siqueira, P.; Simard, M.; Griffith, P. *NACP New England and Sierra National Forests Biophysical Measurements: 2008–2010*. Oak Ridge National Laboratory Distributed Active Archive Center: Oak Ridge, TN, USA, 2011. Available online: <http://dx.doi.org/10.3334/ORNLDAAAC/1046> (accessed on 15 April 2012).
8. Strahler, A.H.; Schaaf, C.; Woodcock, C.; Jupp, D.; Culvenor, D.; Newnham, G.; Dubayah, R.; Yao, T.; Zhao, F.; Yang, X. *ECHIDNA Lidar Campaigns: Forest Canopy Imagery and Field Data, USA, 2007-2009*. Oak Ridge National Laboratory Distributed Active Archive Center: Oak Ridge, TN, USA, 2011. Available online: <http://dx.doi.org/10.3334/ORNLDAAAC/1045> (accessed on 15 April 2012).
9. ECHIDNA Lidar Campaigns: Forest Canopy Imagery and Field Data, USA, 2007-2009. Available online: <http://daac.ornl.gov/NACP/guides/ECHIDNA.html> (accessed on 15 April 2012).
10. Laser Vegetation Imaging Sensor. Available online: <https://lvis.gsfc.nasa.gov/index.php> (accessed on 15 April 2012).
11. Lee, S.; Ni-Meister, W.; Yang, W.Z.; Chen, Q. Physically based vertical vegetation structure retrieval from ICESat data: Validation using LVIS in White Mountain National Forest, New Hampshire, USA. *Remote Sens. Environ.* **2011**, *115*, 2776–2785.
12. *ICESat/GLAS Data—Overview*. Available online: <http://nsidc.org/data/icesat/index.html> (accessed on 15 April 2012).
13. Fry, J.A.; Xian, G.; Jin, S.M.; Dewitz, J.A.; Homer, C.G.; Yang, L.M.; Barnes, C.A.; Herold, N.D.; Wickham, J.D. National land cover database for the conterminous United States. *Photogramm. Eng. Rem. Sensing* **2011**, *77*, 859–864.
14. National Land Cover Database 2006 (NLCD2006). <http://www.mrlc.gov/nlcd2006.php> (accessed on 15 April 2012).

15. Hansen, M.C.; DeFries, R.S.; Townshend, J.R.G.; Carroll, M.; Dimiceli, C.; Sohlberg, R.A. Global percent tree cover at a spatial resolution of 500 meters: First results of the MODIS vegetation continuous fields algorithm. *Earth Int.* **2003**, *7*, 1–10.
16. Simard, M.; Pinto, N.; Fisher, J.B.; Baccini, A. Mapping forest canopy height globally with spaceborne lidar. *J. Geophys. Res-Biogeosci.* **2011**, *116*, doi: 10.1029/2011jg001708.
17. Gesch, D.; Evans, G.; Mauck, J.; Hutchinson, J.; Carswell, W.J. *The National Map—Elevation: U.S. Geological Survey Fact Sheet 2009-3053*; 2009; p. 4. Available online: <http://pubs.usgs.gov/fs/2009/3053/> (accessed on 15 April 2012)
18. Harding, D.J.; Carabajal, C.C. ICESat waveform measurements of within-footprint topographic relief and vegetation vertical structure. *Geophys. Res. Lett.* **2005**, *32*, doi: 10.1029/2005gl023471.
19. Zhang, G.; Ganguly, S.; Nemani, R.; White, M.; Milesi, C.; Wang, W.; Saatchi, S.; Yu, Y.; Myneni, R.B. A simple parametric estimation of live forest aboveground biomass in California using satellite derived metrics of canopy height and Leaf Area Index. *Geophys. Res. Lett.* **2013**, under review.
20. Abshire, J.B.; Sun, X.L.; Riris, H.; Sirota, J.M.; McGarry, J.F.; Palm, S.; Yi, D.H.; Liiva, P. Geoscience Laser Altimeter System (GLAS) on the ICESat mission: On-orbit measurement performance. *Geophys. Res. Lett.* **2005**, *32*, doi: 10.1029/2005gl024028.
21. Chen, Q. Retrieving vegetation height of forests and woodlands over mountainous areas in the Pacific Coast region using satellite laser altimetry. *Remote Sens. Environ.* **2010**, *114*, 1610–1627.
22. Lefsky, M.A.; Keller, M.; Pang, Y.; de Camargo, P.B.; Hunter, M.O. Revised method for forest canopy height estimation from Geoscience Laser Altimeter System waveforms. *J. Appl. Remote Sens.* **2007**, *1*, doi: 10.1117/1.2795724.
23. Pang, Y.; Lefsky, M.; Sun, G.Q.; Ranson, J. Impact of footprint diameter and off-nadir pointing on the precision of canopy height estimates from spaceborne lidar. *Remote Sens. Environ.* **2011**, *115*, 2798–2809.
24. Duncanson, L.I.; Niemann, K.O.; Wulder, M.A. Estimating forest canopy height and terrain relief from GLAS waveform metrics. *Remote Sens. Environ.* **2010**, *114*, 138–154.
25. Sun, G.; Ranson, K.J.; Kimes, D.S.; Blair, J.B.; Kovacs, K. Forest vertical structure from GLAS: An evaluation using LVIS and SRTM data. *Remote Sens. Environ.* **2008**, *112*, 107–117.
26. Neuenschwander, A.L. Evaluation of waveform deconvolution and decomposition retrieval algorithms for ICESat/GLAS data. *Can. J. Remote Sens.* **2008**, *34*, S240–S246.
27. Rosette, J.A.B.; North, P.R.J.; Suarez, J.C.; Los, S.O. Uncertainty within satellite LiDAR estimations of vegetation and topography. *Int. J. Remote Sens.* **2010**, *31*, 1325–1342.